ACS OMEGA

http://pubs.acs.org/journal/acsodf

Article

Lab Case Study of Microbiologically Influenced Corrosion and Rietveld Quantitative Phase Analysis of X-ray Powder Diffraction Data of Deposits from a Refinery

Husam S. Khanfar and Husin Sitepu*

Cite This: *ACS Omega* 2021, 6, 11822−11831

Read Online

ACCESS | Metrics & More | Article Recommendations

ABSTRACT: This paper reports a laboratory-based case study for the characterization of deposits from a crude cooler and reboilers in a Saudi Aramco refinery by microbiologically influenced corrosion (MIC) using microbial, metallurgic, and special analyses and correlates the Rietveld quantitative phase analysis of high-resolution X-ray powder diffraction (XRD) data of scale deposits with microbe compositions. Therefore, rapid in-field microbiological assays could be carried out to assess the potential of MIC. Based on the results, it can be highlighted that the MIC investigation showed that total bacteria and sulfate-reducing bacteria (SRB) were detected in all sampling locations. Methanogens, acid-producing bacteria, and sulfate-reducing archaea were not detected in all samples. Iron-oxidizing bacteria (IOB) were detected in the solid samples from reboilers C and D. Low loads of general bacteria and low levels of microbes with MIC potential were detected in both C and D samples. The trace amount of corrosion products in one sample and the low level of MIC microbes cannot justify the contribution of MIC microbes in the formation of accumulated solids in the system. The findings recommend conducting frequent sampling and analysis including water, oil, and solid from upstream locations to have more decisive evidence of the likelihood of the scale formation and possible contribution of MIC in the formation of deposits in the plant. Subsequently, quantitative phase analysis of XRD data of scale deposits by the Rietveld method revealed that the major phase is calcium sulfate in the form of anhydrate and the minor phases are calcium carbonate in the form of calcite and aragonite, silicon oxide in the form of quartz, and iron oxide corrosion product in the form of magnetite. The results are supported by high-resolution wavelength-dispersive X-ray fluorescence (WDXRF) results. These accurate and reproducible X-ray crystallography findings obtained from Rietveld quantitative phase analysis can guide the field engineers at the refineries and gas plants to overcome the problems of the affected equipment by drawing up the right procedures and taking preventive actions to stop the generation of these particular deposits.

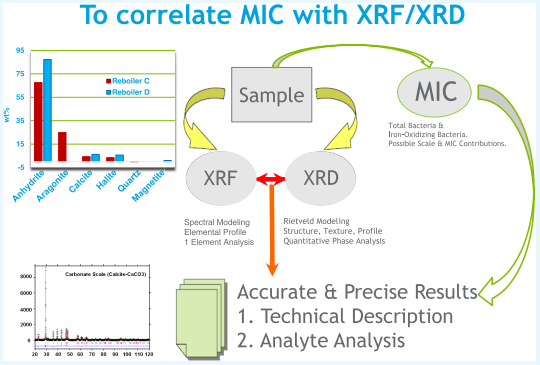

1. INTRODUCTION

Kannan et al.[1] reviewed the analytical methods used for detecting microbiologically influenced corrosion (MIC) in the oil and gas industry and used a combination of morphological, compositional, electrochemical, and biological analyses of 77 studies on MIC. They showed that the microbiological assay techniques (e.g., metagenomics and metabolomics techniques) provide a rapid tool to evaluate MIC of corrosion deposits from refineries and gas plants. Additionally, a laboratory case study of MIC is required to obtain reproducible results and accurately and precisely simulate field conditions. They suggested that one of the keys to rapidly and directly detect the MIC in the affected equipment on-site without transporting the corrosion products to off-field characterization facilities. Additionally, the database will add impact to MIC and can be deployed in the field for biosensor identification, which includes the use of quantitative polymerase chain reaction (qPCR) for key performance indicators.

The accumulated sludge deposits or solid deposits play a destructive role by damaging equipment in oil and gas facilities. Such damage can lead to shutting down of the facilities, which results in loss of production, expensive repairs, and corrective treatment to resume working again efficiently.[2−5] The exchangers are designed as once-through reboilers (see Figure 1). The column bottom temperature is maintained at 95 °C to meet the bottom product specifications. Crude oil return from the

Received: September 29, 2020
Accepted: March 11, 2021
Published: April 26, 2021

ACS Publications

© 2021 American Chemical Society

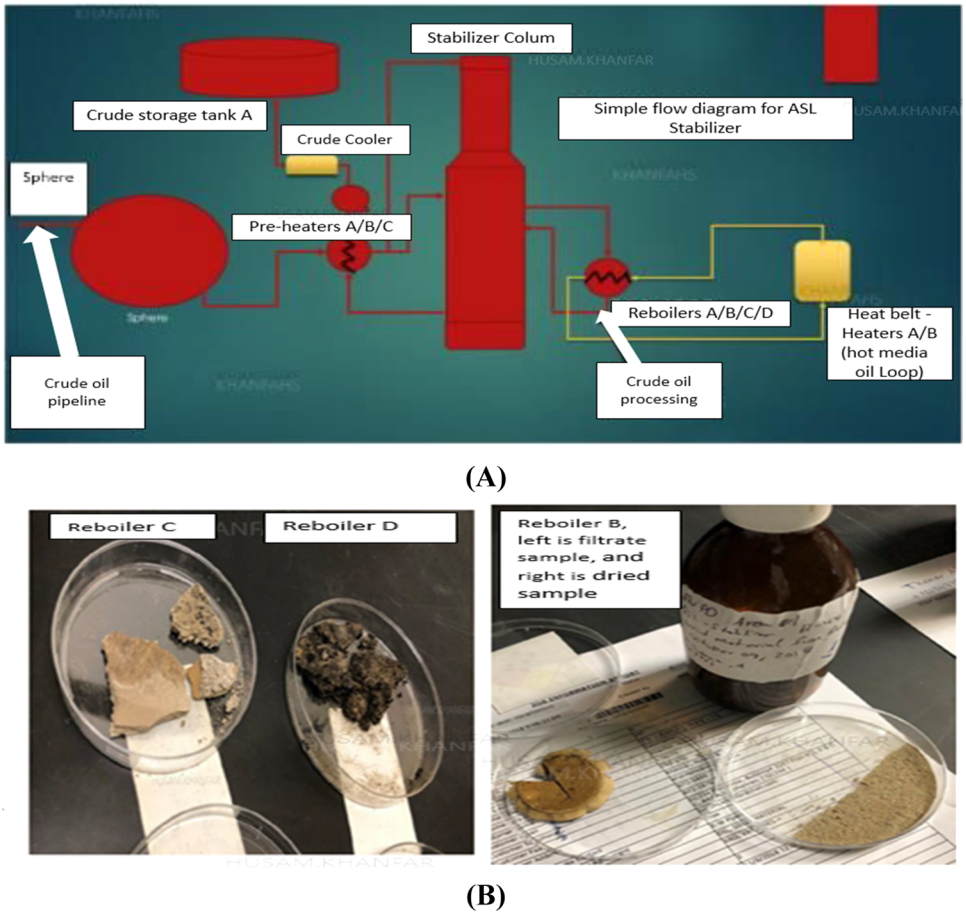

Figure 1. (A) Schematics layout of crude cooler stabilizer reboilers A, B, C, and D. (B) Physical appearance of the deposits collected from reboilers B, C, and D.

reboilers enters the column below the chimney tray. Reboiler-generated vapor travels up the column through the chimney tray risers. Heat is supplied to the stabilizer reboilers by the heating media from a hot belt reboiler system. The stabilizer bottom pumps transfer the stabilized crude oil product from the column bottom on level control and undergo initial cooling by exchanging heat with the column middle feed in the stabilizer feed preheaters. The cooler and the reboilers are not directly connected as per the following functional description.[6,7]

1.1. Crude Cooler. The stabilized crude oil cooler is an air-cooled exchanger, which cools the stabilized crude from the bottom of the stabilizer column before the crude flows to the crude oil storage tanks. The cooler is designed to cool 924 095 kg/h (2 037 260 lb/h) of crude from 122.9 °C (or 253.3 °F) to 56.7 °C (or 134.0 °F) for summer operation and 944 144 kg/h (2 081 460 lb/h) from 92.4 °C (or 198.3 °F) to 25.6 °C (or 78.0 °F) for winter operation.[8]

1.2. Stabilizer Reboilers A/B/C/D. Internal reflux arriving at the bottom of the stabilizer column is collected in the bottom chimney tray and fed to the four (4) stabilizer reboilers. The exchangers are designed as once-through reboilers. The column bottom temperature is maintained at 95 °C (203 °F) to meet the bottom product specifications. Crude oil return from the reboilers enters the column below the chimney tray. Reboiler-generated vapors travel up the column through the chimney tray risers.

Heat is supplied to the stabilizer reboilers by the heating media from the hot belt reboiler system. The stabilizer bottom pumps transfer the stabilized crude oil product from the column bottom on level control and undergo initial cooling by exchanging heat with the column middle feed in the stabilizer feed preheaters. The cooler and the reboilers are not connected, and there are other processes between them.[8]

1.3. Objectives. In this study, the overall objectives of this paper are divided into two parts. Part I is to conduct a laboratory-based case study for the characterization of the deposits from a crude cooler and reboilers in a Saudi Aramco refinery by MIC using microbial, metallurgic, and special analyses; the Karl Fisher moisture test; a sulfur content test; environmental scanning electron microscopy (ESEM); and wavelength-dispersive X-ray fluorescence (WDXRF) spectrometry and correlate the findings to the microbe compositions so that rapid in-field microbiological assays could be carried out to assess the potential of MIC. The additional significantly important objective of Part II is to determine accurately and precisely which phases were involved in the accumulated deposits and their contents quantitatively by Rietveld refinement[9−16] of whole X-ray powder diffraction (XRD) patterns of the inorganic crystalline material part of the deposits.[2−5] The accurate and reproducible X-ray crystallography findings can guide the field engineers at the refineries and gas plants to facilitate efficient cleaning of the equipment by drawing up the right procedures and taking preventive actions to stop the generation of these particular deposits.

https://doi.org/10.1021/acsomega.0c04770
ACS Omega 2021, 6, 11822−11831

2. EXPERIMENTS

2.1. Sampling. Figure 1A shows the one oil sample received from the crude cooler. Subsequently, Figure 1B depicts three solid deposits collected from reboilers B, C, and D. The as-received deposits from reboiler B were oily, and therefore, the authors performed the separation of the inorganic crystalline material part (nonhydrocarbon) of the sludge deposits from the hydrocarbon part.[2−5] The as-received deposits were gray dry from reboiler C and black dry from reboiler D.

In this experiment, the characterizations of these deposits were divided into two parts. Part I is to characterize the deposits by MIC using microbial, metallurgic, and special analyses; the Karl Fisher moisture test; the sulfur content test; ESEM; and WDXRF spectrometry and correlate the X-ray fluorescence (XRF) element concentrations to the microbe compositions so that rapid in-field microbiological assays could be carried out to assess the potential of MIC. Part II is significantly important challenging to determine accurately and precisely quantitative phase analysis of whole X-ray powder diffraction patterns of the inorganic crystalline material part of the deposits by Rietveld refinement, which provide reproducible results and therefore can guide the engineers at the affected refineries and gas plants to overcome the problems by devising the right corrective procedures.

2.2. Part I: Microbiological Analysis, Karl Fisher Moisture Test, Sulfur Content Test, ESEM, and WDXRF Spectrometry. *2.2.1. Microbiological Analysis.* MIC investigation was conducted to determine the load and types of microbes in oil and solid samples using the advanced molecular technique, which is based on molecular microbiology for detection of different of MIC groups, such as total bacteria (BA)[17], sulfate-reducing bacteria (SRB),[18−20] acid-producing bacteria (APB),[20,21] iron-oxidizing bacteria (IOB),[22−24] sulfate-reducing archaea (SRA),[17,24] and methanogens (MET) using the quantitative polymerase chain reaction (qPCR) technique.[25−27]

2.2.2. Oil Sample Special Test Examination by Karl Fisher Moisture Test D-6304 and Sulfur Content Test D-4294. The Karl Fisher moisture test D-4294 method covers the direct determination of water in the range of 10−25 000.00 mg/kg entrained water in petroleum products and hydrocarbons using automated instrumentation. This test method also covers the indirect analysis of water thermally removed from samples and swept with dry inert gas into the Karl Fischer titration cell. Mercaptan, sulfide (S^- or H_2S), sulfur, and other compounds are known to interfere with this test method. This test method is intended for use with commercially available coulometric Karl Fischer reagents and for the determination of water in additives, lube oils, base oils, automatic transmission fluids, hydrocarbon solvents, and other petroleum products. By proper choice of the sample size, this test method may be used for the determination of water from mg/kg to percent-level concentrations.[28−33]

The sulfur content test D-4294 method covers the determination of total sulfur in petroleum and petroleum products that are single-phase and either liquid at ambient conditions, liquefiable with moderate heat, or soluble in hydrocarbon solvents. These materials can include diesel fuel, jet fuel, kerosene, other distillate oil, naphtha, residual oil, lubricating base oil, hydraulic oil, crude oil, unleaded gasoline, gasoline-ethanol blends, biodiesel, and similar petroleum products.[28−33]

2.2.3. ESEM. A field-emission gun environmental scanning electron microscope[1,34−36] was utilized to study the compositional features of the samples. The sample was analyzed using a Quanta 400 ESEM at 20 kV and 10 mm working distance. General compositional images at different magnifications were acquired. In addition, low-resolution energy-dispersive X-ray spectra (EDS) in the spot mode were acquired from different particles to determine the elemental composition of the sample particles.

2.2.4. High-Resolution WDXRF Spectrometry.[37] For WDXRF elemental composition,[37] the as-received samples were manually grounded in an agate mortar and pestle to a fine powder and mixed thoroughly. It is imperative for accurate quantitative analysis that the sample is finely ground and homogeneous.[14,15] Subsequently, 4 g of homogenized sample was mixed well with 0.9 g of binder (Licowax C micropowder PM (Hoechstwax)) using a Spex 8000 mixer/mill. Moreover, the homogenized mixture was pressed at a pressure of 20 tons to form the pellet sample with a diameter of 31 mm. Subsequently, the pellet sample was irradiated with X-ray photons from the X-ray tube. The intensity of the X-rays was processed by the PANalytical WDXRF instrument's software (i.e., Omnian) to determine semiquantitatively the concentrations of the detected elements.

2.3. Part II: Quantitative Phase Analysis by the Rietveld Method. *2.3.1. Qualitative Analysis.* For qualitative analysis (i.e., chemical analysis, or phase identification, or fingerprint) of X-ray powder diffraction (XRD) data, Gates-Rector and Blanton[38] and Fawcett et al.[39] described that the International Centre for Diffraction Data (ICDD) of the powder diffraction file (PDF) database has the primary purpose to (i) serve as a quality reference tool for the powder diffraction community and (ii) edit, publish, and distribute XRD data for the identification of materials. The ICDD-PDF-4+ database consists of the crystallographic information files (CIFs) of crystalline materials that can be used to determine phase identification of powder diffraction data. Jenkins et al.[40] pointed out that since 1941, the PDF has been the primary qualitative crystalline phase identification reference for powder diffraction data. Gates et al.[41] extended the ICDD-PDF database to semicrystalline and amorphous (noncrystalline) materials. The ICDD-PDF database provides the details of the crystal structure of crystalline materials (e.g., space groups, lattice parameters, atomic coordinates, and thermal parameters), which can be used to perform phase identification, quantitative phase analysis,[9−13] crystallographic preferred orientation[2−5,9−16] characterization, and crystal structure refinement by the Rietveld method.[40−52] Therefore, Kuzel and Danis[53] indicated that the ICDD-PDF database and other crystallographic databases are some of the key tools to perform structure refinements in the International of Crystallography (IUCr) Powder Diffraction Community. Gates-Rector and Blanton[38] highlighted that the ICDD-PDF-4+ crystallographic database

(i) consists of structural details and provide the PDF card for the inorganic and organic diffraction data used for phase identification and material characterization by X-ray, synchrotron, and neutron powder diffraction data;

(ii) is editorially reviewed and processed according to ISO 9001:2015, and therefore, this crystallographic database is certified; and

(iii) is both computer- and web-accessible; serves a wide range of disciplines covering academic, industrial, and govern-

https://doi.org/10.1021/acsomega.0c04770
ACS Omega 2021, 6, 11822−11831

Table 1. Types and Counts of MIC Microbes in Oil and Solid Deposits[a]

		microbiologically influenced corrosion results						
deposits from	type of deposits	BA	SRB	SRA	APB	MET	IOB	Unit
crude cooler	oil	6.53×10^3	3.11×10^3	BDL	BDL	BDL	BDL	Cell/L
reboiler B	solid deposits	7.13×10^3	3.37×10^3	BDL	BDL	BDL	BDL	Cell/g
reboiler C	solid deposits	4.99×10^3	6.56×10^2	BDL	BDL	BDL	8.00×10^2	Cell/g
reboiler D	solid deposits	1.12×10^3	3.37×10^3	BDL	BDL	BDL	8.10×10^2	Cell/g

[a]BA, total bacteria; SRB, sulfate-reducing bacteria; SRA, sulfate-reducing archaea; APB, acid-producing bacteria; MET, methanogens; IOB, iron-oxidizing bacteria; and BDL, below detection limit.

ment laboratories; and describes in detail the content of database entries presented to enhance the use of the PDF.

For XRD data measurements, the as-received deposits were manually ground by an agate mortar and a pestle for several minutes to achieve a fine particle size.[14,15] Then, the fine powders were mounted into the sample holders of the Rigaku Ultima IV XRD by front pressing. To perform the chemical analysis in this study, the authors used HighScore Plus software[54] and combined with the International Powder Diffraction Data (ICDD, 2018)[38,55] of the powder diffraction file (PDF-4+) database of the standard reference materials, which is an excellent analytical technique used for the phase identification of XRD data.[38−53] Importantly, the phase identification of XRD data of the very small crystalline inorganic part materials can accurately be used to differentiate between different forms of calcium carbonate ($CaCO_3$) scale formation materials (e.g., calcite or scale deposits (aragonite) or vaterite) that have different crystal structures.[2] Additionally, the iron sulfide corrosion products that appear in the very small quantities of the crystalline inorganic part materials of the sludge deposits have a wide range of chemical compositions and different crystalline structures, for example, marcasite (orthorhombic), greigite (cubic), and mackinawite (tetragonal).[2]

2.3.2. Quantitative Phase Analysis of Whole X-ray Powder Diffraction Pattern by the Rietveld Method. Quantitative analysis[9−13] (phase composition or wt %), i.e., W_p, of each of the identified phases, p, is proportional to the product of the scale factor, s, as derived in the Rietveld refinement, with the mass and volume of the unit cell according to

$$W_p = s_p(ZMV)_p / \sum_{i=1}^{n} s_i(ZMV)_i$$

where Z is the number of formula units per unit cell, M is the mass of the formula unit, and V is the unit cell volume (in Å^3), respectively. The advantages of this quantitative phase analysis by the Rietveld method compared to the conventional reference intensity ratio method[9−16] are that quantitative phase analysis by the Rietveld method provides (i) accurate and precise results without the need for complex procedures of laborious experimental calibration and is (ii) 30 000 times quicker than the reference intensity ratio method.

2.3.3. Reproducibility of XRD Phase Identification and Quantifications by the Rietveld Method. Scarlett et al.[13] described that one of the main sources of error to perform accurate quantitative phase analysis of high-quality high-resolution XRD data by the Rietveld method is microabsorption, which is the presence of absorption contrast between phases. In some circumstances, they showed that microabsorption proves to be challenging. In this paper, the limited amount of inorganics deposits (i.e., nonhydrocarbon parts) were manually ground in an agate mortar and a pestle for several minutes to achieve fine particle size[14−16] and eliminate microabsorption effects. To reproduce the results, the sample preparations were carefully repeated—the size distribution of the limited amount of inorganic deposits was modified by McCrone micronizing mill to achieve inadequate intensity reproducibility.[15,16] Excellent agreement was obtained between the results of the two experiments (i.e., McCrone mill-micronizing and manually ground in an agate mortar and a pestle) and following O'Connor et al.[14]—the microabsorption correction was not conducted—in refinement. The results of the manually ground in an agate mortar and a pestle for several minutes are quoted here as the experimental data of the limited amount of the inorganic crystalline material part of the sludge deposits were of superior quality in terms of counting statistics.

3. RESULTS AND DISCUSSION

3.1. Part I: Experimental Results. *3.1.1. Microbiological Analysis.* The as-received four samples were subjected to microbiological investigation using the quantitative polymerase chain reaction (qPCR) technique to determine the microbes with MIC potential, as indicated in Table 1. The results of the oil sample type collected from crude cooler indicated total bacteria (BA) and sulfate-reducing bacteria (SRB) up to 10^3 cell/L. Additionally, the corresponding results for the solid deposits from reboilers B, C, and D indicated total bacteria and sulfate-reducing bacteria up to 10^3 cell/L, iron-oxidizing bacteria (IOB) up to 10^2 cell/g in both deposits from reboilers C and D, and below detection limit (BDL) in oily sludge deposits from the crude cooler and reboiler B. Note that the sulfate-reducing archaea (SRA), methanogens (MET), and acid-producing bacteria (APB) were not detected in all samples.

Table 1 shows that the sum of sulfate-reducing bacteria and iron-oxidizing bacteria is 1.456×10^3 for the deposits from the reboiler C sample and 4.580×10^3 for the deposits from the reboiler D sample. Additionally, the total bacterial count is 4.99×10^3 for the deposits from reboiler C and 1.12×10^3 for the deposits from reboiler D. It means that the total bacterial count divided by the sum of sulfate-reducing bacteria and iron-oxidizing bacteria is 3.427 for the deposits from the reboiler C sample and 0.245 for the deposits from reboiler D. So, the total bacterial count divided by the sum of sulfate-reducing bacteria and iron-oxidizing bacteria value for the deposits from reboiler C is approximately 14× bigger than the corresponding value for the deposits from reboiler D.

In deposits from reboiler D, sulfate-reducing archaea more than total bacteria results, there are different factors which can be experimentally the sources of the systematics errors because of the following reasons:

- The authors use a TaqMan probe in the total bacteria protocol along with primers to target 16s RNA, while in

https://doi.org/10.1021/acsomega.0c04770
ACS Omega 2021, 6, 11822−11831

the sulfate-reducing bacteria, SYBER green is used to detect a functional gene.

- The target of the total quantitative bacteria polymerase chain reaction is the V6 region of the 16S rRNA gene. Bacteria contain a median of three copies of the 16S rRNA gene per genome.
- The target of sulfate-reducing quantitative bacteria polymerase chain reaction is dissimilatory sulfite reductase subunit α and β (dsrAB) gene. Sulfate-reducing bacteria contain a single copy of the dsrAB gene per genome.
- The gene copy number of 16s RNA is contained to be a medium number around three, and therefore, the calculation will be different based on the population target, while the gene copy in the functional gene is usually one.
- The optimization process of the quantitative bacteria polymerase chain reaction protocol is different: each protocol stands alone; the total bacteria is one protocol and the plasmid standard design based on one mesophilic, spore-forming, thermophilic stain, whereas the sulfate-reducing bacteria protocol is three protocols calculated as total sulfate-reducing bacteria and the plasmid design contain three mesophilic, spore-forming, thermophilic microorganisms.
- In this study, the authors deal with environmental samples from the field, and therefore, sometimes DNA extraction efficiency varied in the species of a group of microorganisms that can experimentally play a role.

3.1.2. Oil Sample Special Test Examination. The oily deposits from the crude cooler were subjected to the special test of the Karl Fisher moisture test, which mainly determines the trace amounts of water in the oily sample using the ASTM D-6304 standard. The results obtained from the Karl Fisher moisture test D-6304 for the oily sample from the crude cooler revealed that the crude oil sample consists of 111.5 parts per million (ppm), see Table 2. Subsequently, the sulfur content (wt %) test of the oily sample was conducted using the ASTM D-4294 standard, which yields a fast analysis technique for the accurate determination of sulfur in petroleum derivatives. The results obtained from test D-4294 for the oily sample from the crude cooler revealed that sulfur content is 0.032 wt %, see Table 3.

Table 2. Summary of the Result Obtained from the Karl Fisher Moisture Test D-6304 for the Oily Sample from the Crude Cooler

analytical method	trace amounts of water (ppm)
Karl Fischer moisture test ASTM D-6304	111.5

3.1.3. ESEM and EDS Analyses. Figure 2A,B depicts the ESEM compositional "Z-contrast" images acquired using a solid-state electron backscattered detector. The acquired ESEM image characterization data showed that the solid deposit from reboiler B is composed of highly agglomerated microscopic particles. The corresponding ESEM energy-dispersive X-ray micromeasurements revealed that solid deposits from reboiler B comprise C, O, Na, Mg, Si, S, Cl, and Ca (Figure 2A), which suggests that scale formation has taken place in the equipment. Nonetheless, this requires further investigation to determine the likelihood of scale formation and decide the appropriate remedial actions. However, the filtered deposits from reboiler B showed the presence of different irregularly shaped microscopic particles (Figure 2A). Furthermore, EDS analyses in the spot mode showed that some of the particles were rich in Fe oxide and others consisted of Na and Cl. The high level of C (Figure 2A) may be due to the presence of hydrocarbons and also from the filter paper too. Figure 3A,B shows the presence of varying levels of Ca, C, O, S, Cl, Na, and Fe and traces of Mg, Si, Al, and K elements in deposits from reboilers C and D.

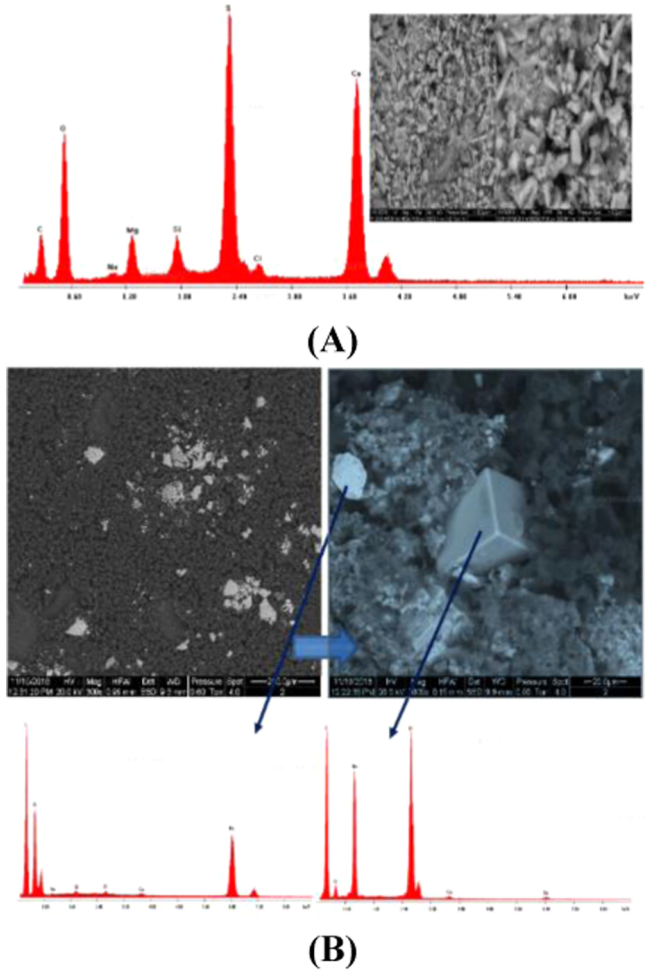

Figure 2. ESEM images and corresponding EDS spectra for the deposit from reboiler B in (A) general area analysis mode and (B) spot analysis mode (left) from Fe-rich solid particles and (right) salt-rich particles from the filtrate sample.

Table 3. Summary of the Sulfur Content (wt %) Result for the Oily Sample from the Crude Cooler Obtained from Sulfur Content Test D-4294

analytical method	sulfur content (wt %)
sulfur test ASTM D-4294	0.032

It must be clarified that the estimated error in the performed low-resolution energy-dispersive spectrometry (EDS) analyses is ±5 to 10% and higher for trace elements (less than 1 wt %). There is a possible source of errors in the data due to peak overlapping, absorption, and ESEM low-resolution energy-dispersive spectrometry. The limitation of the ESEM and EDS is that it has low resolution and can only be used to determine the

https://doi.org/10.1021/acsomega.0c04770
ACS Omega 2021, 6, 11822−11831

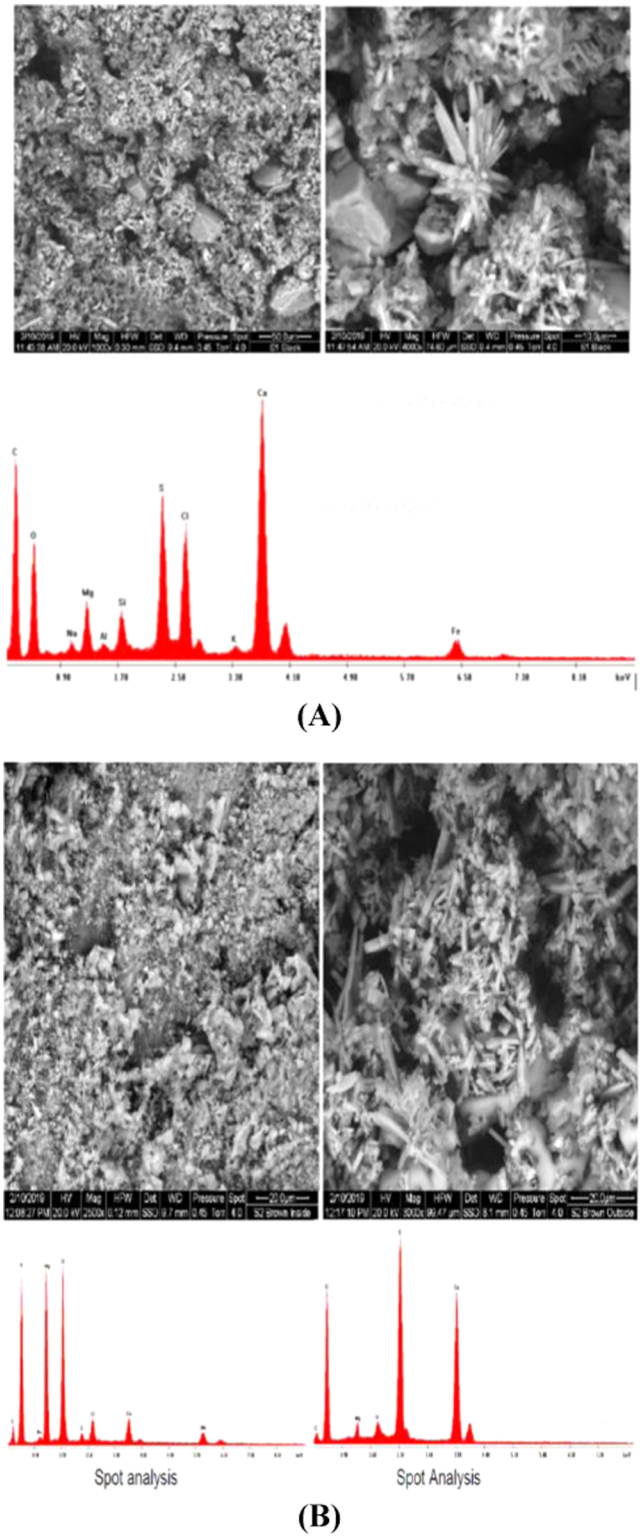

Figure 3. ESEM surface topographical images and corresponding EDS spectra for deposits from reboilers C and D in (A) general area analysis mode and (B) spot analysis mode.

elements present in a certain location of the samples semiquantitatively.

The authors therefore independently determined the elements and their concentrations in the deposits from reboilers B, C, and D by high-resolution wavelength-dispersive X-ray fluorescence (WDXRF) spectrometry and instrument software (i.e., Omnian), see the below section. The WDXRF results along with the phase identification of XRD data and quantitative phase analysis of the identified phase obtained by the Rietveld method, which are accurate and reproducible results, are given below.

3.1.4. Measured Elements and Their Contents Obtained from PANalytical Advanced AXIOS WDXRF Spectrometry Calculated by the Instrument's Standardless Software (i.e., Omnian). The elements appearing in the specific area of the solid samples in reboilers C and D were originally investigated using the low-resolution energy-dispersive spectra (EDS-ESEM). Subsequently, the high-resolution WDXRF spectrometry and its software (i.e., Omnian) were used to determine the elements and their concentrations semiquantitatively. Furthermore, the qualitative phase analysis (i.e., phase composition or chemical composition) of the XRD data of crystalline materials was conducted by combining HighScore Plus Software and ICDD-PDF+4 software.

The detected Ca, C, O, S, Cl, Na, Fe, and traces of Mg, Si, Al, and K elements in deposits from reboilers C and D by ESEM images/EDS spectra were unquantified. Therefore, the contents of each of the detected elements by high-resolution PANalytical Advanced AXIOS WDXRF spectrometry were independently and semiquantitatively calculated by the instrument's standardless software (i.e., Omnian), see Figure 4. It can be clearly

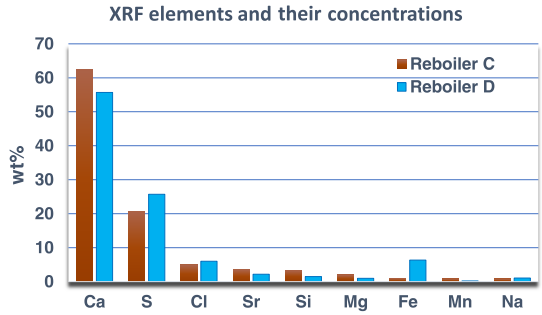

Figure 4. Variation between the elements and their concentrations obtained from high-resolution WDXRF spectrometry and the instrument's standardless software (i.e., Omnian) for deposits from both reboilers C and D.

seen from Figure 4 that the high-resolution WDXRF spectra showed that the major elements are Ca and S and the minor elements are Cl, Sr, Si, Mg, Fe, Mn, and Na. The Ca element is formed from water. To speed up the phase identification of the XRD data, these detected elements by XRF were included as the chemistry restrictions during the search match using the combined HighScore Plus Software and ICDD-PDF-4+ software, see the below section.

The basic principles of the physics of WDXRF and ESEM-EDS spectrometry show no substantial difference, whereas for quantification purposes, WDXRF is always better mainly because it has a much better energy/wavelength resolution and peak/background ratio than that of ESEM-EDS. Energy shifts (chemical shifts) are determined by interaction of electrons with specimens, and therefore, WDXRF provides better accuracy and precision than those of WDXRF-EDS. It means that when the reasonably well quantification of elements is required, WDXRF should be used if it is available. Note that WDXRF is highly sensitive to topography;[37] it means that slight changes in the specimen height can lead to significant changes in the intensity.

https://doi.org/10.1021/acsomega.0c04770
ACS Omega 2021, 6, 11822−11831

3.1.5. Qualitative Analysis and Quantitative Phase Analysis of Whole-Powder Diffraction Patterns by the Rietveld Method. Note that XRD phase identification or fingerprinting is a qualitative method, in which the XRD pattern of the samples was compared with every calculated pattern in the ICDD-PDF-4+ database.[32−49] Using the search-match capabilities of HighScore Plus software and the ICDD-PDF database, all crystalline phases present in the samples were identified. The measured XRD patterns showed that the filter sample (top) hat consists of the amorphous with the small additional of crystalline, whereas the XRD pattern of the very small quantities of the inorganic deposits part of sludge deposits from reboiler B are mixed between the crystalline materials and amorphous. Subsequently, the XRD data sets of crystalline materials were carefully, accurately, and precisely identified by HighScore Plus software (X'Pert HighScore Plus Version 4.8, PANalytical Inc.) using the chemistry restrictions from WDXRF results, see Figure 5. The results for deposits from reboiler B showed that inorganic

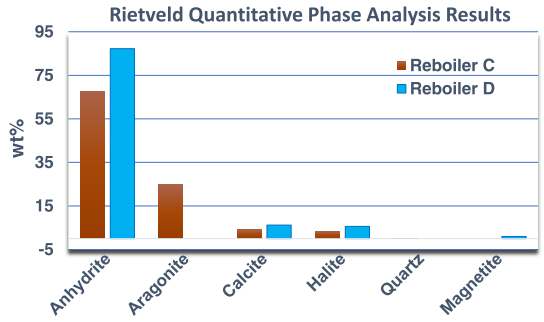

Figure 5. Quantitative phase analysis of the very small amount of the crystalline material parts of the deposits both from reboilers C and D obtained from the Rietveld method.

crystalline materials consist of anhydrite ($CaSO_4$); calcium carbonate ($CaCO_3$) in the form of calcite, aragonite, and dolomite [$CaMg(CO_3)_2$]; sodium chlorite in the form of halite (NaCl) and silicon oxide in the form of quartz (SiO_2).

In X-ray crystallography, Rietveld quantitative phase analysis (or phase composition) means the weight percentage for each of the identified crystalline materials (i.e., they are summed to 100.00%).[2−5,9−16] The major phase (i.e., the highest weight percentage for all of the identified phases) obtained from the Rietveld method is anhydrate, which shows that the reboiler D sample is higher than that of the corresponding value for the reboiler C sample.

Note that all of the X-ray powder diffraction (XRD) data were collected at room temperature. Additionally, the most important is that the phase identification of XRD data of the crystalline material part of the deposits can accurately be used to differentiate between different forms of calcium carbonate ($CaCO_3$) scale formation materials (e.g., calcite or scale deposits (aragonite)) that have different crystal structures:

- calcite has a hexagonal structure with the space group of $R\bar{3}c$ (no. 167) and cell parameters of $a = b = 4.988$ Å, $c = 17.068$ Å, $\alpha = \beta = 90°$, and $\gamma = 120°$;[2,15,16]
- aragonite has an orthorhombic structure with the space group of *Pnam* (no. 62) and cell parameters of $a = 5.743$ Å, b = 7.969 Å, $c = 4.962$ Å, and $\alpha = \beta = \gamma = 90°$;[2] and
- vaterite has a hexagonal structure with the space group of $P6_3/mmc$ (no. 194) and cell parameters of $a = b = 4.130$ Å, $c = 8.490$ Å, $\alpha = \beta = 90°$, and $\gamma = 120°$.[2]

The source of the Ca element in the XRF spectra is water. This Ca element from XRF (Section 3.1.4) forms calcium carbonate ($CaCO_3$) compounds in XRD findings.

When combined HighScore Plus Software and ICDD-PDF-4+ software were used to identify the measured XRD data, it is an excellent analytical technique used for the phase identification of a crystalline material in scale deposits, catalysts, chemicals, cores, shells, clay minerals, and cement.[2−5] Importantly, it can be used to identify chemical compounds (e.g., $CaCO_3$, NaCl, Si, etc.), whereas other complementary techniques with their software, such as X-ray fluorescence, inductively coupled plasma mass spectrometry, and atomic absorption spectroscopy techniques, can only be used to identify elements (e.g., Na, Ca, Si, etc.) and not chemical compounds.[2−5] An additional advantage of the phase identification of XRD data with combined HighScore Plus Software and ICDD-PDF-4+ software[38−55] compared to the other analytical techniques is that the phase identification results can be used to differentiate accurately between different forms of a chemical compound with the same chemical formula.[2−5] For example, calcite, aragonite, and vaterite have the same chemical formula ($CaCO_3$), but they have different crystallographic structures. That means a sample that has the same chemical formula, calcium carbonate ($CaCO_3$), can be identified as scale formation materials, e.g., calcite, or scale deposits (aragonite) or vaterite. Moreover, iron sulfides that are formed have a wide range of chemical compositions and different crystalline structures can be identified as, for example, pyrite (FeS_2), marcasite (FeS_2), mackinawite ($FeS_{0.9}$), pyrrhotite (Fe_7S_8), and greigite (Fe_3S4). It is very important to know the form of an iron sulfide because some of these iron sulfides are pyrophoric, presenting a risk of ignition. Furthermore, the phase identification results of the XRD data can also differentiate among the hydration states of the compounds in the sample, for example, distinguishing gypsum ($CaSO_4{\cdot}2H_2O$) from both basanite ($CaSO_4{\cdot}0.5H_2O$) and anhydrite ($CaSO_4$).[2]

When the Rietveld method[9−16] was used to quantify the whole X-ray powder diffraction pattern (see Sections 2.3.2 and 2.3.3), the results revealed that the major phase is anhydrite ($CaSO_4$) with the addition of calcite ($CaCO_3$), aragonite ($CaCO_3$), halite (NaCl), quartz (SiO_2), and dolomite ($CaMg(CO_3)_2$), see Figure 5. The findings are supported by the XRF results (see Figure 4).

3.2. Discussions. *3.2.1. Part I.* Investigations into the microbiologically influenced corrosion (Figure 1 and Table 1) showed the presence of total bacteria and sulfate-reducing bacteria in all samples from crude oil and deposits from reboiler B, reboiler C, and reboiler D. However, the sulfate-reducing archaea, acid-producing bacteria, and methanogens were not detected in all samples. Note that the iron-oxidizing bacteria were only detected in the deposits from reboilers C and D. Based on microbiologically influenced corrosion risk threshold, the crude oil, and considered a medium microbiologically influenced corrosion, whereas the deposits from reboiler B, reboiler C, and reboiler D exhibited medium microbiologically influenced corrosion risk. It is interesting to note that the ESEM image of deposits from reboiler B showed that the solid deposits are composed of highly agglomerated microscopic particles. For oil sample special test examination, it can be highlighted that although dissolved water seriously damages the lubricating properties of oil and promotes component corrosion, increased water concentrations (>500 ppm) indicate possible condensation, coolant leakage, or process leakage around the seals, and

https://doi.org/10.1021/acsomega.0c04770
ACS Omega 2021, 6, 11822−11831

low levels of dissolved water by the Karl Fischer test indicate low concentrations (111 ppm). Additionally, corrosive sulfur and the effect are already known and can be significant. The extent of corrosion damage caused by sulfur, if left unchecked, can be so severe as to cause the failure of the apparatus. The result of the sulfur content was in a low range of 0.032 wt % in this study, and such a percentage has no direct or immediate effect on corrosion. For ESEM and low-resolution EDS study, the results suggested that scale formation has taken place in the equipment. In contrast, the filtrated deposits from reboiler B showed the presence of different irregularly shaped microscopic particles (Figures 2 and 3). The element concentration (wt %)[37] obtained from high-resolution PANalytical Advanced AXIOS WDXRF spectrometry and the instrument's standardless software (i.e., Omnian) revealed that the major elements are Ca and S and the minor elements are Cl, Sr, Si, Mg, Fe, Mn, and Na (Figure 4). The Ca element is formed from water.

3.2.2. Part II. The elemental compositions obtained from high-resolution PANalytical Advanced AXIOS WDXRF spectrometry and Omnian software were used as restrictions in qualitative analysis (i.e., phase identification) of the high-resolution X-ray powder diffraction (XRD) data of the small amount of crystalline material part of the deposits.[2−5] The XRD patterns of the deposits from reboiler B are amorphous, which cannot be identified. The XRD data of the deposits from reboiler C and reboiler D showed that they are crystalline materials. When the XRD data of the crystalline material part of the deposits from reboiler C and reboiler D were identified by combined HighScore Plus and ICDD-PDF-4+, the results revealed that the data consist of anhydrite ($CaSO_4$), calcite ($CaCO_3$), aragonite ($CaCO_3$), halite (NaCl), quartz (SiO_2), and dolomite ($CaMg(CO_3)_2$). Subsequently, when Rietveld refinement was used to determine quantitative phase analysis of the identified phases,[9−16] the results indicated that the major phase is anhydrite with the addition of calcite, aragonite, halite, quartz, and dolomite phases, see Figure 5. The findings are supported by the elemental composition (wt %)[37] results obtained from WDXRF spectrometry and Omnian software (Figure 4) for deposits from both reboilers C and D. Therefore, the Rietveld quantitative phase analysis results can guide the engineers at the affected refineries and gas plants to overcome the problems by devising the appropriate corrective procedures.[2−5]

When the results obtained from microbiologically influenced corrosion investigation were correlated with the Rietveld quantitative phase analysis of high-resolution X-ray powder diffraction (XRD) data of the crystalline material part of scale deposits from both reboilers C and D, it can be highlighted these deposits contained compounds of anhydrite ($CaSO_4$), calcite ($CaCO_3$), aragonite ($CaCO_3$), halite (NaCl), quartz (SiO_2), and dolomite ($CaMg(CO_3)_2$), which shows high levels of Ca element from XRF. However, XRD shows low levels of microbes with microbiologically influenced corrosion potential with the small addition of corrosion products in the form of magnetite (Fe_3O_4) for the deposits from reboiler D only. Therefore, it is not likely that microbiologically influenced corrosion microbes contributed to the formation of the accumulated solids in the system. To have more decisive evidence of the origin of scales and the possible contribution of microbiologically influenced corrosion in the formation of deposits in the refineries and gas plants, frequent sampling and Rietveld quantitative phase analysis[9−16] from upstream locations are recommended to be conducted.

4. CONCLUSIONS

In the present study, the authors (i) conducted a laboratory-based case study for the characterization of corrosion deposits from a crude cooler and reboilers in a Saudi Aramco refinery by microbiologically influenced corrosion (MIC) using microbial, metallurgic, and special analyses and (ii) correlate the Rietveld quantitative phase analysis of high-resolution X-ray powder diffraction (XRD) data of scale deposits to the microbe compositions so that rapid in-field microbiological assays could be carried out to assess the potential of MIC. Based on the results, it can be concluded that the

- MIC investigation showed that the total bacteria and sulfate-reducing bacteria (SRB) were detected in all sampling locations. Methanogens, acid-producing bacteria, and sulfate-reducing archaea were not detected in all samples. Iron-oxidizing bacteria (IOB) were detected in the solid samples from reboilers C and D.
- Low loads of general bacteria and low levels of microbes with MIC potential were detected in both C and D samples. The trace amount of corrosion products in one sample and the low level of MIC microbes cannot justify the contribution of MIC microbes in the formation of the accumulated solids in the system.
- The MIC findings recommend conducting frequent sampling and analysis including water, oil, and solid from upstream locations to have more decisive evidence of the likelihood of the scale formation and possible contribution of MIC in the formation of solid deposits in the plant.
- Quantitative phase analysis by the Rietveld method revealed that the major phase is calcium sulfate in the form of anhydrate and the minor phases are calcium carbonate in the form of calcite and aragonite, silicon oxide in the form of quartz, and the iron oxide corrosion product in the form of magnetite. The results are supported by the high-resolution wavelength-dispersive X-ray fluorescence (WDXRF) results.
- These accurate and reproducible X-ray crystallography findings can guide the field engineers at the refineries and gas plants to overcome the problems of the affected equipment by drawing up the right procedures and taking preventive actions to stop the generation of these particular deposits.

AUTHOR INFORMATION

Corresponding Author

Husin Sitepu − *Saudi Aramco, Research and Development Center, Dhahran 31311, Saudi Arabia*; Email: sitepuhx@aramco.com

Author

Husam S. Khanfar − *Saudi Aramco, Research and Development Center, Dhahran 31311, Saudi Arabia*; orcid.org/0000-0002-4377-2356

Complete contact information is available at: https://pubs.acs.org/10.1021/acsomega.0c04770

Notes

The authors declare no competing financial interest.

https://doi.org/10.1021/acsomega.0c04770
ACS Omega 2021, 6, 11822−11831

■ ACKNOWLEDGMENTS

The authors acknowledge the Saudi Aramco R&DC management for giving permission to publish the results. Thanks are also due to Yazeed Al-Dukhayyil of TSD Divison Head, Mazen Al-Saleh Supervisor of AMU, and Salman J. Al-Khaldi Supervisor of AAU for their encouragement. Thanks are also due to all TSD employees who helped and encouraged this study, and without their help, this paper would not be possible. Also, special thanks are given to Ammar S. Alsaqer, Abdulkareem M. Alqahtani, Fares Z. Abo Ali, Hameed Al-Badairy, Akram A. Alfillow, Noktan M. AlYami, and Abdullah K. Dakheel.

■ REFERENCES

(1) Kannan, P.; Su, S. S.; Mannan, M. S.; Castaneda, H.; Vaddiraju, S. A Review of Characterization and Quantification Tools for Microbiologically Influenced Corrosion in the Oil and Gas Industry: Current and Future Trends. *Ind. Eng. Chem. Res.* **2018**, *57*, 13895−13922.

(2) Sitepu, H. Rietveld Phase Analysis of Deposits Formed at Different Locations within Electric Submersible Pump's Parts. *Adv. X-Ray Anal.* **2020**, *63*, 28−42.

(3) Sitepu, H.; Al-Ghamdi, R. A. Quantitative Phase Analysis of XRD Data of Sludge Deposits from Refineries and Gas Plants by Use of the Rietveld Method. *Adv. X-Ray Anal.* **2019**, *62*, 45−57.

(4) Sitepu, H.; Al-Ghamdi, R. A.; Zaidi, S. R. Corrigendum to Application of a New Method in Identifying the Sludge Deposits from Refineries and Gas Plants: A Case of Laboratory-Based Study. *Int. J. Corros.* **2018**, No. 8646104.

(5) Sitepu, H.; Zaidi, S. R. Application of a New Method in Identifying the Sludge Deposits from Refineries and Gas Plants: A Case of Laboratory-Based Study. *Int. J. Corros.* **2017**, No. 9047545.

(6) Kakaç, S.; Liu, H.; Pramuanjaroenkij, A. *Heat Exchangers: Selection, Rating, and Thermal Design*; CRC Press: Boca Raton, FL, 2012.

(7) Faes, W.; Lecompte, S.; Ahmed, Z.; Van Bael, J.; Salenbien, R.; Verbeken, K.; De Paepe, M. Corrosion and Corrosion Prevention in Heat Exchangers. *Corros. Rev.* **2019**, *37*, 131−155.

(8) Kushwaha, D. K.; Kundnaney, N. D. In *A Critical Review on Heat Exchangers Used in Oil Refinery*, Afro-Asian International Conference on Science, Engineering & Technology 2015; GEC Bharuch, 2015.

(9) Hill, R. J.; Howard, C. J. Quantitative Phase Analysis from Neutron Powder Diffraction Data Using the Rietveld Method. *J. Appl. Crystallogr.* **1987**, *20*, 467−474.

(10) O'Connor, B. H.; Raven, M. D. Application of the Rietveld Refinement Procedure in Assaying Powdered Mixtures. *Powder Diffr.* **1988**, *3*, 2−6.

(11) Bish, D. L.; Howard, S. A. Quantitative Phase Analysis Using the Rietveld Method. *J. Appl. Crystallogr.* **1988**, *21*, 86−91.

(12) Hill, R. J. Expanded Use of the Rietveld Method in Studies of Phase Mixtures. *Powder Diffr.* **1991**, *6*, 74−77.

(13) Scarlett, N. V. Y.; Madsen, I. C. Quantification of Phases with Partial or No Known Crystal Structure. *Powder Diffr.* **2006**, *21*, 278−284.

(14) O'Connor, B. H.; Li, D. Y.; Sitepu, H. Strategies for preferred orientation corrections in X-ray powder diffraction using line intensity ratios. *Adv. X-Ray Anal.* **1991**, *34*, 409−415.

(15) Sitepu, H.; O'Connor, B. H.; Li, D. Y. Comparative Evaluation of the March and Generalized Spherical Harmonic Preferred Orientation Models Using X-ray Diffraction Data for Molybdite and Calcite Powders. *J. Appl. Crystallogr.* **2005**, *38*, 158−167.

(16) Sitepu, H. Texture and Structural Refinement Using Neutron Diffraction Data from Molybdite (MoO_3) and Calcite ($CaCO_3$) Powders and a Ni-rich $Ni_{50.7}Ti_{49.30}$ Alloy. *Powder Diffr.* **2009**, *24*, 315−326.

(17) Zhu, X. Y.; Modi, H.; Ayala, A.; Kilbane, J. J. Rapid Detection and Quantification of Microbes Related to Microbiologically Influenced Corrosion Using Quantitative Polymerase Chain Reaction. *Corrosion* **2006**, 950−955.

(18) Little, B.; Lee, J. *Microbiologically Influenced Corrosion Hoboken*; John Wiley & Sons: NJ, 2007; p 272.

(19) Javaherdashti, R. *Microbiologically Influenced Corrosion: An Engineering Insight*; Springer-Verlag: London, UK, 2008; p 172.

(20) Jørgensen, B. B. Mineralization of Organic Matter in the Sea Bed − the Role of Sulphate Reduction. *Nature* **1982**, *296*, 643−645.

(21) Zhang, T.; Fang, H. H. P.; Ko, B. C. B. Methanogen Population in a Marine Biofilm Corrosive to Mild Steel. *Appl. Microbiol. Biotechnol.* **2003**, *63*, 101−106.

(22) Lee, J. S.; McBeth, J. M.; Ray, R. I.; Little, B. J.; Emerson, D. Iron Cycling at Corroding Carbon Steel Surfaces. *Biofouling* **2013**, *29*, 1243−1252.

(23) Ray, R. I.; Lee, J. S.; Little, B. J.; Gerke, T. L. The Anatomy of Tubercles: A Corrosion Study in a Fresh Water Estuary. *Mater. Corros.* **2010**, *61*, 993−999.

(24) Hubert, C.; Voordouw, G. Oil Field Souring Control by Nitrate-Reducing Sulfur Spirillum Spp. that Outcompete Sulfate-Reducing Bacteria for Organic Electron Donors. *Appl. Environ. Microbiol.* **2007**, *73*, 2644−2652.

(25) Davidova, I. A.; Duncan, K. E.; Perez-Ibarra, B. M.; Suflita, J. M. Involvement of thermophilic archaea in the biocorrosion of oil pipelines. *Environ. Microbiol.* **2012**, *14*, 1762−1771.

(26) Mori, K.; Tsurumaru, H.; Harayama, S. Iron corrosion activity of anaerobic hydrogen-consuming microorganisms isolated from oil facilities. *J. Biosci. Bioeng.* **2010**, *110*, 426−430.

(27) Mand, J.; Park, H. S.; Jack, T. R.; Voordouw, G. The Role of Acetogens in Microbially Influenced Corrosion of Seel. *Front. Microbiol.* **2014**, *5*, No. 268.

(28) Bansal, B.; Müller-Steinhagen, H.; Chen, X. D. Effect of suspended particles on crystallization fouling in plate heat exchangers. *J. Heat Transfer* **1997**, *119*, 568−574.

(29) Andritsos, N.; Karabelas, A. J. The influence of particulates on $CaCO_3$ scale formation. *J. Heat Transfer* **1999**, *121*, 225−227.

(30) Hasson, D.; Sherman, H.; Biton, M. In *Predictions of CaCO3 Scaling Rates*, Proceedings of 6th International Symposium Fresh Water from the Sea, 1978; pp 193−199.

(31) Karabelas, A. J. Scale formation in tubular heat exchangers—research priorities. *Int. J. Therm. Sci.* **2002**, *41*, 682−692.

(32) ASTM D6304 - 20. Standard Test Method for Determination of Water in Petroleum Products, Lubricating Oils, and Additives by Coulometric Karl Fischer Titration. https://www.astm.org/Standards/D6304.htm (Retrieved June 3, 2020).

(33) ASTM D4294-16e1. Standard Test Method for Sulfur in Petroleum and Petroleum Products by Energy Dispersive X-ray Fluorescence Spectrometry. https://www.astm.org/Standards/D4294.htm (Retrieved June 3, 2020).

(34) Bache, I. C.; Donald, A. The Structure of the Gluten Network in Dough: a Study using Environmental Scanning Electron Microscopy. *J. Cereal Sci.* **1998**, *28*, 127−133.

(35) Kirk, S. E.; Skepper, J. N.; Donald, A. M. Application of Environmental Scanning Electron Microscopy to Determine Biological Surface Structure. *J. Microsc.* **2009**, *233*, 205−224.

(36) Esmaily, M.; Svensson, J. E.; Fajardo, S.; Birbilis, N.; Frankel, G. S.; Virtanen, S.; Arrabal, R.; Thomas, S.; Johansson, L. G. Fundamentals and Advances in Magnesium Alloy Corrosion. *Prog. Mater. Sci.* **2017**, *89*, 92−193.

(37) Sitepu, H.; Kopylopa, M. G.; Quirt, D. H.; Cutler, J. N.; Kotzer, T. G. Synchrotron micro-X-ray Fluorescence Maps of Natural Diamonds: First Steps in Identification of Mineral Inclusions In-situ. *Am. Mineral.* **2005**, *90*, 1740−1747.

(38) Gates-Rector, S.; Blanton, T. The Powder Diffraction File: A Quality Materials Characterization Database. *Powder Diffr.* **2019**, *34*, 352−360.

(39) Fawcett, T. G.; Kabekkodu, S. N.; Blanton, J. R.; Blanton, T. N. Chemical Analysis by Diffraction: the Powder Diffraction File. *Powder Diffr.* **2017**, *32*, 63−71.

(40) Jenkins, R.; Holomany, M.; Wong-Ng, W. On the Need for Users of the Powder Diffraction File to Update Regularly. *Powder Diffr.* **1987**, *2*, 84−87.

https://doi.org/10.1021/acsomega.0c04770
ACS Omega 2021, 6, 11822−11831

(41) Gates, S. D.; Blanton, T. N.; Fawcett, T. G. A New 'Chain' of Events: Polymers in the Powder Diffraction File (PDF). *Powder Diffr.* **2014**, *29*, 102−107.
(42) Belsky, A.; Hellenbrandt, M.; Karen, V. L.; Luksch, P. New Developments in the Inorganic Crystal Structure Database (ICSD): Accessibility in Support of Materials Research and Design. *Acta Crystallogr., Sect. B: Struct. Sci.* **2002**, *58*, 364−369.
(43) Downs, R.; Hall-Wallace, M. The American Mineralogist Crystal Structure Database. *Am. Mineral.* **2003**, *88*, 247−250.
(44) Gražulis, S.; Daškevič, A.; Merkys, A.; Chateigner, D.; Lutterotti, L.; Quirós, M.; Serebryanaya, N. R.; Moeck, P.; Downs, R. T.; Le Bail, A. Crystallography Open Database (COD): an Open-Access Collection of Crystal Structures and Platform for World-Wide Collaboration. *Nucleic Acids Res.* **2012**, *40*, D420−D427.
(45) Bruno, I.; Gražulis, S.; Helliwell, J. R.; Kabekkodu, S. N.; McMahon, B.; Westbrook, J. Crystallography and Databases. *Data Sci. J* **2017**, *16*, 1−17.
(46) Faber, J.; Fawcett, T. The Powder Diffraction File: Present and Future. *Acta Crystallogr., Sect. B: Struct. Sci.* **2002**, *B58*, 325−332.
(47) Groom, C. R.; Bruno, I. J.; Lightfoot, M. P.; Ward, S. C. The Cambridge Structural Database. *Acta Crystallogr., Sect. B: Struct. Sci., Cryst. Eng. Mater.* **2016**, *B72*, 171−179.
(48) Villars, P.; Cenzual, K. *Pearson's Crystal Data, Crystal Structure Database for Inorganic Compounds*; ASM International: Materials Park, Ohio, USA, 2017.
(49) Hanawalt, J. D.; Rinn, H. W.; Frevel, L. K. Chemical Analysis by X-ray Diffraction. *Ind. Eng. Chem., Anal. Ed.* **1938**, *10*, 457−512.
(50) Jenkins, R.; Smith, D. "The Powder Diffraction File", *IUCr Data Base Commission Report, August 1987*; Allen, F. H.; Bergerhoff, G.; Sievers, R., Eds.; Data Commission of the International Union of Crystallography: UK, 1987; pp 158−177.
(51) Messick, J. The History of the International Centre for Diffraction Data. *Powder Diffr.* **2012**, *27*, 36−44.
(52) Smith, D.; Jenkins, R. The Powder Diffraction File: Past, Present, and Future. *J. Res. Natl. Inst. Stand. Technol.* **1996**, *101*, 259−271.
(53) Kuzel, R.; Danis, S. Structural Databases of Inorganic Materials. *Mater. Struct.* **2007**, *14*, 89−96.
(54) Degen, T.; Sadki, M.; Bron, E.; König, U.; Nénert, G. The HighScore Suite. *Powder Diffr.* **2014**, *29*, S13−S18.
(55) *PDF-4+ 2018 (Database)*; Kabekkodu, S., Ed. International Centre for Diffraction Data: Newtown Square, PA, USA, 2018.

https://doi.org/10.1021/acsomega.0c04770
ACS Omega 2021, 6, 11822−11831